



Submitted to

International Europhysics Conference on High Energy Physics, EPS03, July 17-23, 2003, Aachen
(Abstract **087** Parallel Session **5**)

XXI International Symposium on Lepton and Photon Interactions, LP03, August 11-16, 2003, Fermilab

www-h1.desy.de/h1/www/publications/conf/conf_list.html

Dijets in Diffractive Photoproduction at HERA

H1 Collaboration

Abstract

A measurement is presented of differential dijet cross sections in low- $|t|$ diffractive photoproduction processes of the type $ep \rightarrow eXY$, in which the photon dissociation system X is separated from a leading low-mass baryonic system Y by a large rapidity gap. The measurement is based on an integrated luminosity of 18 pb^{-1} . Dijet events are identified using the inclusive k_T cluster algorithm. The cross sections are given at the level of stable hadrons and correspond to the kinematic range $Q^2 < 0.01 \text{ GeV}^2$, $165 < W < 240 \text{ GeV}$, $x_{IP} < 0.03$, $E_T^{\text{jet}1} > 5 \text{ GeV}$ and $E_T^{\text{jet}2} > 4 \text{ GeV}$. The measurements are compared with predictions based on diffractive parton distributions obtained from a QCD analysis of inclusive diffractive DIS and with diffractive dijet production in DIS.

1 Introduction

An open task in high energy physics is to obtain a consistent understanding of diffractive hadronic scattering observed in different processes. Theoretically it is expected that the cross section σ_{incl}^D for inclusive diffractive deep-inelastic scattering (DIS) factorises into universal diffractive parton distributions and process dependent hard scattering coefficients [1]. Diffractive parton densities have been determined from DGLAP QCD fits to inclusive diffractive HERA data [2, 3] and have been found to be dominated by the gluon distribution. Diffractive dijet production in DIS [4] is directly sensitive to the gluon component of the diffractive exchange and is in good agreement with the QCD fits to the inclusive diffractive data. However, applying the diffractive parton densities to predict diffractive dijet production at the Tevatron, leads to an overestimation of the observed rate by one order of magnitude [5]. This discrepancy has been attributed to the presence of the additional beam hadron remnant in $p\bar{p}$ collisions which leads to secondary interactions and a break-down of factorisation. The suppression, often characterised by a reduced ‘rapidity gap survival probability,’ cannot be calculated perturbatively and has been parameterised in various ways (see, e.g., [6]).

The transition from DIS to hadron-hadron scattering can be studied in photoproduction at HERA, where the beam lepton emits a quasi-real photon which interacts with the proton. Processes in which a real photon participates directly in the hard scattering are expected to be similar to deep-inelastic scattering of highly virtual photons. In contrast, processes in which the photon is first resolved into partons which then initiate the hard scattering resemble hadron-hadron scattering. Via resolved photon processes in hard photoproduction, parton final states are accessible, which are present in the equivalent $p\bar{p}$ collisions but not in DIS. Different prescriptions for diffraction can therefore be tested in the regime of hard diffractive photoproduction.

In this paper, a measurement of diffractive dijet cross sections in photoproduction is presented, based on data collected with the H1 detector at HERA. The integrated luminosity is increased by one order of magnitude with respect to previous results [7]. Jets are defined using the inclusive k_T cluster algorithm with asymmetric cuts on the jet transverse energies to facilitate future comparisons with next-to-leading order calculations. The cross sections are compared with diffractive dijet production in DIS and with predictions based on diffractive parton distributions obtained from inclusive ep scattering.

2 Kinematics

Figure 1a shows the generic diffractive process $ep \rightarrow eXY$, in which the systems X and Y are by definition separated by the largest rapidity gap in the hadronic final state, and Y is the proton system. Figure 1b shows a resolved photon diffractive dijet process. The beam lepton emits a quasi-real photon which interacts with the proton, leading to the formation of two jets within the X system.

With k and P denoting the momenta of the incoming electron¹ and proton, respectively, and q the momentum of the photon, kinematic variables are defined:

$$s \equiv (k + P)^2; \quad Q^2 \equiv -q^2; \quad y \equiv \frac{q \cdot P}{k \cdot P}. \quad (1)$$

¹Throughout the paper, the word ‘electron’ is used synonymously for positrons.

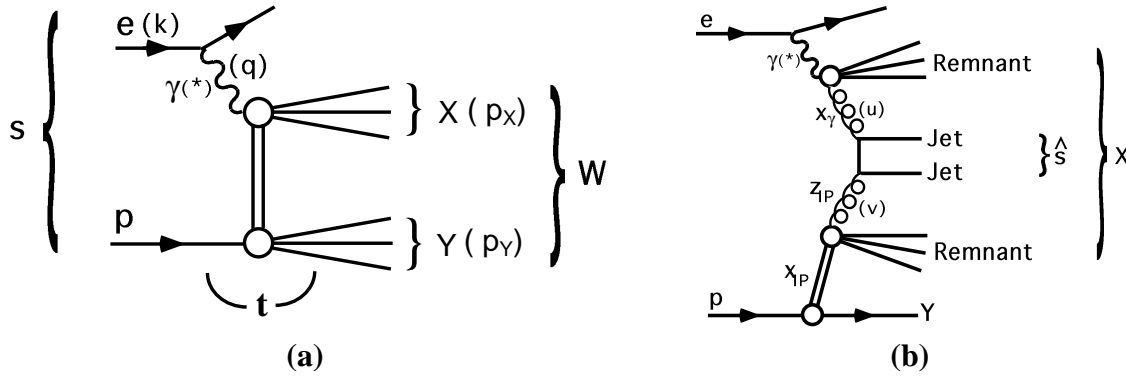


Figure 1: (a) The generic process $ep \rightarrow eXY$, in which the diffractive system X is separated from the proton system Y by the largest rapidity gap in the final state particle distribution. (b) A resolved photon process of diffractive dijet production, viewed in terms of the Resolved Pomeron model.

y is related to the γp centre-of-mass energy $W = \sqrt{y s}$. With p_X and p_Y representing the momenta of the systems X and Y , the data are discussed in terms of

$$M_X^2 \equiv p_X^2; \quad M_Y^2 \equiv p_Y^2; \quad t \equiv (P - p_Y)^2; \quad x_{IP} \equiv \frac{q \cdot (P - p_Y)}{q \cdot P}. \quad (2)$$

M_X and M_Y are the invariant masses of the systems X and Y , t is the squared 4-momentum transferred between the incoming proton and the photon, and x_{IP} is the fraction of the proton beam momentum transferred to the system X . With u and v denoting the momenta of the partons entering the hard subprocess from the photon and the proton, respectively (as indicated in Figure 1b), the dijet system has squared invariant mass

$$\hat{s} = M_{12}^2 = (u + v)^2. \quad (3)$$

The longitudinal fractional momenta carried by the partons from the photon and the diffractive exchange are given by

$$x_\gamma = \frac{P \cdot u}{P \cdot q}; \quad z_P = \frac{q \cdot v}{q \cdot (P - p_Y)}. \quad (4)$$

3 Diffractive Parton Distributions

In [2, 3] diffractive parton distributions of the proton have been determined through DGLAP QCD fits to inclusive diffractive DIS data. The fits were made under the additional assumptions that the shapes of the parton distributions do not depend on x_{IP} and their normalisation is controlled through Regge phenomenology (resolved pomeron model [8]). These assumptions are consistent with the present data. In [2], the leading order (LO) fits which gave the best description of the data are referred to as ‘H1 fit 2’ and ‘H1 fit 3.’ Cross sections for diffractive dijet production in DIS have been presented in [4]. The dijet rate in diffractive DIS depends strongly on the diffractive gluon distribution via boson-gluon fusion. It has been demonstrated in [4]

that diffractive dijet production in DIS is described to within 10% by the parton distributions corresponding to ‘H1 fit 2’ of the inclusive analysis. The data themselves have an uncertainty of about 20%. The H1 fit 2 parton densities have also been used to predict diffractive dijet production at the Tevatron. There, the measured diffractive structure function of the anti-proton is overestimated by approximately one order of magnitude [5].

DGLAP QCD fits to new high precision data for inclusive diffractive DIS data have been presented in [3]. The obtained LO parton distributions lead to an underestimation of the dijet rate in DIS of about 20% when p_T is used as the hard scale. These LO parton densities are referred to as ‘H1 2002 fit’ in the present paper.

The diffractive parton densities can also be used to predict diffractive dijet cross sections in direct and resolved photoproduction, where the jet transverse momentum is used for the renormalisation and factorisation scale and the photon and pomeron parton distributions are convoluted with standard partonic cross sections. Up to now, predictions for dijet rates, based on diffractive parton distributions and the resolved pomeron model, can only be made in LO QCD and are subject to large scale uncertainties and model assumptions. It is therefore useful to compare the dijet rate in photoproduction with both the new H1 2002 fit to the recent precise inclusive DIS data and, as directly as possible, to the dijet rate in DIS. The latter can be done by looking at the ratios of expectations to data in DIS and photoproduction, or alternatively, by considering H1 fit 2 as an approximation to the DIS diffractive dijet data within the LO resolved pomeron model. Note, however, that this comparison suffers from slightly different kinematic regions and different jet algorithms used for DIS and photoproduction.

4 Monte Carlo Simulations

In the analysis different Monte Carlo programs were used to correct the data for detector inefficiencies and migrations, and to compare the measured cross sections with model predictions. The RAPGAP 2.08 Monte Carlo program [9] is used to obtain predictions based on diffractive parton densities extracted in inclusive diffractive DIS within the resolved pomeron model. Leading order matrix elements for the hard QCD $2 \rightarrow 2$ subprocess are convoluted with parton distributions of the pomeron and the photon, taken at the scale $\mu^2 = \hat{p}_T^2 + m_{q\bar{q}}^2$, where \hat{p}_T is the transverse momentum of the emerging hard partons and $m_{q\bar{q}}$ is the mass of the produced quarks. For the resolved photon component, the leading order GRV parton distribution functions [10] are used, which were found to give a good description of the effective photon structure function as measured by H1 [11].

For the diffractive exchange, the H1 fit 2 parameterisations are used to simulate pomeron and sub-leading reggeon exchange, which contributes at the highest $x_{\mathcal{P}}$. To avoid divergences in the calculation of the matrix elements, a cut $\hat{p}_T > 2$ GeV is applied on the generator level. No significant losses are seen for the selected jets with $E_T^{\text{jet}1} > 5$ GeV and $E_T^{\text{jet}2} > 4$ GeV due to this cut. Higher order effects are simulated using parton showers [12] in the leading $\log(\mu)$ approximation (MEPS), and the Lund string model [13] is used for hadronisation. RAPGAP does not include remnant interactions. The PYTHIA 6.1 Monte Carlo program [14] is used to simulate inclusive dijet photoproduction processes in order to evaluate migrations from high M_Y and high $x_{\mathcal{P}}$.

5 Experimental Procedure

5.1 H1 Detector

A detailed description of the H1 detector can be found in [15]. Here, a brief account of the components most relevant to the present analysis is given. The H1 coordinate system convention defines the outgoing proton beam direction as the positive z axis and the polar scattering angle θ such that the pseudorapidity $\eta = -\ln \tan(\theta/2)$ increases along z .

The hadronic final state X is measured with a tracking and a calorimeter system. The central ep interaction region is surrounded by two large concentric drift chambers, located inside a 1.15 T solenoidal magnetic field. Charged particle momenta are measured in the range $-1.5 < \eta < 1.5$ with a resolution of $\sigma/p_T = 0.01 p_T/\text{GeV}$. A finely segmented electromagnetic and hadronic liquid argon calorimeter (LAr) covers the range $-1.5 < \eta < 3.4$. The energy resolution is $\sigma/E = 0.11/\sqrt{E/\text{GeV}}$ for electromagnetic showers and $\sigma/E = 0.50/\sqrt{E/\text{GeV}}$ for hadrons, as measured in test beams. A lead/scintillating fibre calorimeter (SPACAL) covers the backward region $-4 < \eta < -1.4$.

The forward region is covered by the Forward Muon Detector (FMD) and the Proton Remnant Tagger (PRT). The 3 pre-toroid drift chambers of the FMD are used to detect particles directly in the region $1.9 < \eta < 3.7$, and from larger pseudorapidities via beam-pipe scattering. The PRT consists of a set of scintillators surrounding the beam pipe at $z = 26$ m and covers the region $6 < \eta < 7.5$.

The ep luminosity is measured via the Bethe-Heitler Bremsstrahlung process $ep \rightarrow ep\gamma$, the final state electron and photon being detected in crystal calorimeters at $z = -33$ m (electron detector) and $z = -103$ m (photon detector), respectively.

5.2 Event Selection

The data used in this analysis were taken in the 1996 and 1997 running periods, in which HERA collided 820 GeV protons with 27.5 GeV positrons. The data are collected using a trigger which requires the scattered electron to be measured in the electron detector and at least 3 tracks in the central jet chamber. The geometrical acceptance of the electron detector limits the measurement to $Q^2 < 0.01 \text{ GeV}^2$ and $0.3 < y < 0.65$. A veto cut requiring less than 2 GeV of deposited energy in the photon detector suppresses accidental coincidences with Bremsstrahlung events.

Rapidity gap events are selected by requiring the absence of activity in the forward direction. No signals above noise levels are allowed in the FMD and PRT. In the LAr, no cluster with an energy of more than 400 MeV is allowed in the region $\eta > 3.2$. These selection criteria ensure that the gap between the systems X and Y spans at least the region $3.2 < \eta < 7.5$, and that $M_Y < 1.6 \text{ GeV}$ and $-t < 1 \text{ GeV}^2$. A cut $x_P < 0.03$ further reduces non-diffractive contributions.

Jets are formed from the tracks and clusters of the hadronic final state X , using the inclusive k_T cluster algorithm [16] (with a distance parameter of 1.0) in the laboratory frame. At least 2 jets are required, with transverse energies $E_T^{\text{jet}1} > 5 \text{ GeV}$ and $E_T^{\text{jet}2} > 4 \text{ GeV}$ for the leading and subleading jet, respectively. The jet axes are required to lie within the region $-1 < \eta_{\text{jet}}^{\text{lab}} < 2$, well within the acceptance of the LAr calorimeter.

5.3 Kinematic Reconstruction

The energy E'_e of the scattered electron is measured directly in the small scattering angle electron detector and is used to reconstruct the fractional photon energy

$$y = E_\gamma/E_e = 1 - E'_e/E_e, \quad (5)$$

where E_e is the electron beam energy. The hadronic system X , containing the jets, is measured in the LAr and SPACAL calorimeters and the central tracking system. Calorimeter cluster energies and track momenta are combined using algorithms which avoid double counting [17]. $x_{\mathcal{P}}$ is reconstructed according to

$$x_{\mathcal{P}} = \frac{\sum_X (E + p_z)}{2 E_p}, \quad (6)$$

in which E_p denotes the proton beam energy and the sum runs over all objects in the X system. The invariant mass of the dijet system is given by

$$M_{12} \equiv \sqrt{(p_{\text{jet1}} + p_{\text{jet2}})^2}, \quad (7)$$

with p_{jet1} and p_{jet2} being the 4-momenta of the leading and sub-leading jet, respectively. The estimators x_γ^{jets} and $z_{\mathcal{P}}^{\text{jets}}$ on the fractional momenta of the partons entering the hard subprocess are reconstructed as:

$$x_\gamma^{\text{jets}} = \frac{\sum_{\text{jets}} (E - p_z)}{2 y E_e}; \quad z_{\mathcal{P}}^{\text{jets}} = \frac{\sum_{\text{jets}} (E + p_z)}{2 x_{\mathcal{P}} E_p}. \quad (8)$$

The invariant mass of the hadronic system M_X is reconstructed according to

$$M_X = \sqrt{\frac{M_{12}^2}{z_{\mathcal{P}}^{\text{jets}} x_\gamma^{\text{jets}}}}. \quad (9)$$

Cross sections are also measured differentially in the transverse momentum of the leading jet p_T^{jet1} , the mean pseudorapidity $\langle \eta_{\text{jet}}^{\text{lab}} \rangle$ of the leading and sub-leading jet, and the jet separation $|\Delta \eta_{\text{jet}}|$:

$$\langle \eta_{\text{jet}}^{\text{lab}} \rangle \equiv \frac{1}{2} (\eta_{\text{jet1}}^{\text{lab}} + \eta_{\text{jet2}}^{\text{lab}}); \quad |\Delta \eta_{\text{jet}}| \equiv |\eta_{\text{jet1}}^{\text{lab}} - \eta_{\text{jet2}}^{\text{lab}}|. \quad (10)$$

$|\Delta \eta_{\text{jet}}|$ is related to the scattering angle in the centre-of-mass system of the hard subprocess.

5.4 Cross Section Measurement

The measured cross sections are defined at the level of stable hadrons. The data are corrected for detector inefficiencies and migrations of kinematic quantities in the reconstruction using the RAPGAP Monte Carlo program. For generated diffractive events, the H1 detector response is simulated in detail and the Monte Carlo events are subjected to the same analysis chain as the data. The simulation gives a good description of the shapes of all data distributions.

Cross Section Definition

$0.3 < y < 0.65$ $Q^2 < 0.01 \text{ GeV}^2$
$N_{\text{jet}} \geq 2$ $E_T^{\text{jet}1} > 5 \text{ GeV}$ $E_T^{\text{jet}2} > 4 \text{ GeV}$ $-1 < \eta_{\text{jet}(1,2)}^{\text{lab}} < 2$
$x_P < 0.03$ $M_Y < 1.6 \text{ GeV}$ $-t < 1 \text{ GeV}^2$

Table 1: The kinematic domain in which the cross sections are measured. The jets are reconstructed using the inclusive k_T algorithm with the distance parameter set to 1.0.

According to the simulations, the detector level observables are well correlated with the hadron level quantities.

The kinematic region for which the cross sections are measured is given in Table 1. The cross sections are presented in terms of a model independent definition of diffraction, where the two hadronic systems X and Y are separated by the largest gap in rapidity in the hadronic final state. Migrations from large M_Y and x_P are corrected for using PYTHIA. Smearing across $M_Y = 1.6 \text{ GeV}$ is evaluated with the DIFFVM [18] simulation of proton dissociation.

An analysis of systematic uncertainties has been performed in which the sensitivity of the measurement to variations of the detector calibration and the Monte Carlo Models used for correction are evaluated. The dominant systematic error on the cross sections arises from the uncertainty in the LAr calorimeter energy scale.

6 Results

In Figures 2–6, differential cross sections are presented in the kinematic range specified in Table 1. The figures also show the predictions of the RAPGAP model using LO diffractive parton densities obtained in DGLAP QCD fits to inclusive diffractive DIS data. The predictions are based on the new H1 2002 fit as the best representation of recent inclusive diffraction data [3] and on H1 fit 2, which gives a good description of diffractive DIS dijet data [4].

All predictions are made using the LO GRV photon parton distributions [10], which describe photon structure measurements well [11]. Variations of the renormalisation and factorisation scale μ by a factor 2 and 0.5 lead to changes in the predicted cross sections of about 20%. The parameterisation of the photon structure has been varied within the experimental constraints, leading to negligible changes of the predicted cross sections.

For the model predictions based on the new H1 2002 fit parton densities, α_s is calculated with $\Lambda_{\text{QCD}} = 0.2 \text{ GeV}$ for 4 flavours. The same value was used in the QCD fit extraction of the

corresponding parton densities in [3]. For the model predictions based on H1 fit 2, the same α_s is used as in the comparison with diffractive DIS dijets in [4].

In a previous contributed conference paper [19], the values used for the strong coupling constant α_s in the model predictions were erroneously taken to be too large. The calculations of the matrix elements for the $2 \rightarrow 2$ hard parton scattering cross section and the parton shower cascade were affected, resulting in predicted dijet cross sections which were too large by a factor of approximately 1.4. This mistake has been corrected for the predictions shown here.

6.1 Dependence on fractional momenta $z_{\mathbb{P}}$, x_γ and $x_{\mathbb{P}}$

The cross section differential in the estimator $z_{\mathbb{P}}^{\text{jets}}$ of the fractional parton momentum from the diffractive exchange is presented in Figure 2. The new H1 2002 fit gives a good description of the diffractive photoproduction dijets. The RAPGAP prediction based on the H1 fit 2 parton densities overestimates the normalisation of the data by a factor ≈ 1.4 .

Figure 3 shows the cross section differential in the estimator x_γ^{jets} of the fractional photon momentum taking part in the hard scattering. The prediction based on the parton densities from the new H1 2002 fit is also shown. The contribution from direct photon processes ($x_\gamma^{\text{true}}=1$) is indicated by the hatched histogram. These interactions dominate the dijet cross section for $x_\gamma^{\text{jets}} > 0.6$. The sum of resolved and direct photon processes in the model gives a good description of the data both in normalisation and in shape throughout the x_γ^{jets} range. There is thus no evidence for any suppression of the diffractive cross section in the region dominated by resolved photons, as might be expected on the basis of data from the Tevatron [5] or phenomenological models [6].

In Figure 4, the normalised differential cross section is shown as function of $x_{\mathbb{P}}$. The H1 2002 fit prediction is shown for different values of the pomeron intercept. While the extreme choice of $\alpha_{\mathbb{P}}(0)=1.4$ is disfavoured, the data are compatible with $\alpha_{\mathbb{P}}(0)=1.17$ and $\alpha_{\mathbb{P}}(0)=1.08$. The small ($\approx 5\%$) contribution from the sub-leading reggeon exchange is also shown.

6.2 Dependence on other variables

The normalised differential cross section is studied for further variables in Figures 5 and 6. The dependence on y is shown in Figure 5a. The predictions from the H1 2002 fit and H1 fit 2 are very similar and describe the data well. The normalised cross section differential in the transverse momentum p_T^{jet1} of the leading jet is shown in Figure 5b. Both H1 fits give similar predictions, which describe the data well. Normalised cross sections differential in M_X , M_{12} , $\langle \eta_{\text{jet}}^{\text{lab}} \rangle$ and $|\Delta \eta_{\text{jet}}|$ are shown in Figures 5c, 5d, 6a and 6b, respectively. As for y and p_T^{jet1} , the shapes of the data are well described by the predictions based on the parton densities from the H1 QCD fits.

6.3 Ratio of dijet cross sections in diffractive photoproduction and DIS

In this section, a comparison is made between diffractive dijet cross sections in DIS and in photoproduction. As shown above, the γp and DIS cross sections can be described well in shape for all variables using the same LO diffractive parton densities. The ratio of expectation to data for photoproduction is found to be a factor 1.3 ± 0.3 (exp.) larger than the same ratio in DIS, where the uncertainty is estimated using the total experimental errors of both measurements. The deduced factor is independent of the diffractive parton distributions used in the comparison. It is, however, obtained using the LO resolved pomeron model and the error does not take into account uncertainties due to the different kinematic ranges and jet algorithms.

At the present level of accuracy, no significant suppression of the diffractive dijet cross section in photoproduction is observed. This result for diffractive photoproduction dijets is to be compared with a suppression factor of about 10 for single diffractive dijet production at the Tevatron [5].

7 Summary

Cross sections are presented for the diffractive production of two jets in the photoproduction regime $Q^2 < 0.01 \text{ GeV}^2$. Compared with previous measurements, the luminosity is increased by one order of magnitude to $L = 18 \text{ pb}^{-1}$. The inclusive k_T algorithm is used to select events with at least 2 jets with transverse energies larger than 5 GeV and 4 GeV. Differential cross sections are measured for various characteristic variables.

Diffractive parton densities determined in a recent H1 QCD fit to inclusive diffractive deep-inelastic scattering data lead to predictions for diffractive dijet photoproduction which describe the shapes and normalisation of the data remarkably well.

The photoproduction data are also compared with dijet production in diffractive DIS using a leading order calculation based on the resolved pomeron model to relate the two measurements. The ratio of expectation to data for photoproduction is found to be a factor 1.3 ± 0.3 (exp.) larger than the same ratio in DIS. This factor does not significantly deviate from unity at the present level of precision and there is no evidence that it differs between direct and resolved photon processes.

At the present level of experimental and theoretical uncertainties, a consistent description of dijets in diffractive DIS and photoproduction is obtained using diffractive parton densities determined in QCD fits to inclusive diffractive DIS data.

Acknowledgements

We are grateful to the HERA machine group whose outstanding efforts have made and continue to make this experiment possible. We thank the engineers and technicians for their work in constructing and now maintaining the H1 detector, our funding agencies for financial support, the DESY technical staff for continual assistance, and the DESY directorate for the hospitality which they extend to the non DESY members of the collaboration.

References

- [1] J. Collins, Phys. Rev. **D57** (1998) 3051 and erratum-ibid. **D61** (2000) 019902.
- [2] H1 Collaboration, C. Adloff *et al.*, Z. Phys. **C76** (1997) 613.
- [3] H1 Collaboration, paper 980 submitted to 31. Intl. Conf. on High Energy Physics, ICHEP 2002, Amsterdam.
- [4] H1 Collaboration, C. Adloff *et al.*, Eur. Phys. J. **C20** (2001) 29.
- [5] CDF Collaboration, T. Affolder *et al.*, Phys. Rev. Lett. **84** (2000) 5043.
- [6] E. Gotsman, E. Levin, U. Maor, Phys. Lett. **B438** (1998) 229;
B. Cox, J. Forshaw, L. Lönnblad, [hep-ph/9908464];
A. Kaidalov, V. Khoze, A. Martin, M. Ryskin, [hep-ph/0306134].
- [7] H1 Collaboration, C. Adloff *et al.*, Eur. Phys. J. **C6** (1999) 421.
- [8] G. Ingelman, P. Schlein, Phys. Lett. **B152** (1985) 256.
- [9] H. Jung, Comp. Phys. Commun. **86** (1995) 147.
- [10] M. Glück, E. Reya, A. Vogt, Phys. Rev. **D46** (1992) 1973;
M. Glück, E. Reya, A. Vogt, Phys. Rev. **D45** (1992) 3986.
- [11] H1 Collaboration, C. Adloff *et al.*, Phys. Lett. **B483** (2000) 36.
- [12] M. Bengtsson, T. Sjöstrand, Z. Phys. **C37** (1988) 465.
- [13] T. Sjöstrand, Comp. Phys. Commun. **39** (1986) 347;
T. Sjöstrand, M. Bengtsson, Comp. Phys. Commun. **43** (1987) 367.
- [14] T. Sjöstrand *et al.*, Comp. Phys. Commun. **135** (2001) 238.
- [15] H1 Collaboration, I. Abt *et al.*, Nucl. Instrum. Methods **A386** (1997) 310 and 348.
- [16] S. Ellis, D. Soper, Phys. Rev. **D48** (1993) 3160;
S. Catani, Y. Dokshitzer, M. Seymour, B. Webber, Nucl. Phys. **B406** (1993) 187.
- [17] H1 Collaboration, C. Adloff *et al.*, Z. Phys. **C74** (1997) 221.
- [18] B. List, Diploma Thesis, Techn. Univ. Berlin, Germany, (1993), unpublished;
B. List, A. Mastroberardino, *DIFFVM: A Monte Carlo Generator for diffractive processes in ep scattering* in *Monte Carlo Generators for HERA Physics*, A. Doyle, G. Grindhammer, G. Ingelman, H. Jung (eds.), DESY-PROC-1999-02 (1999) 396.
- [19] H1 Collaboration, paper 987 submitted to 31. Intl. Conf. on High Energy Physics, ICHEP 2002, Amsterdam.

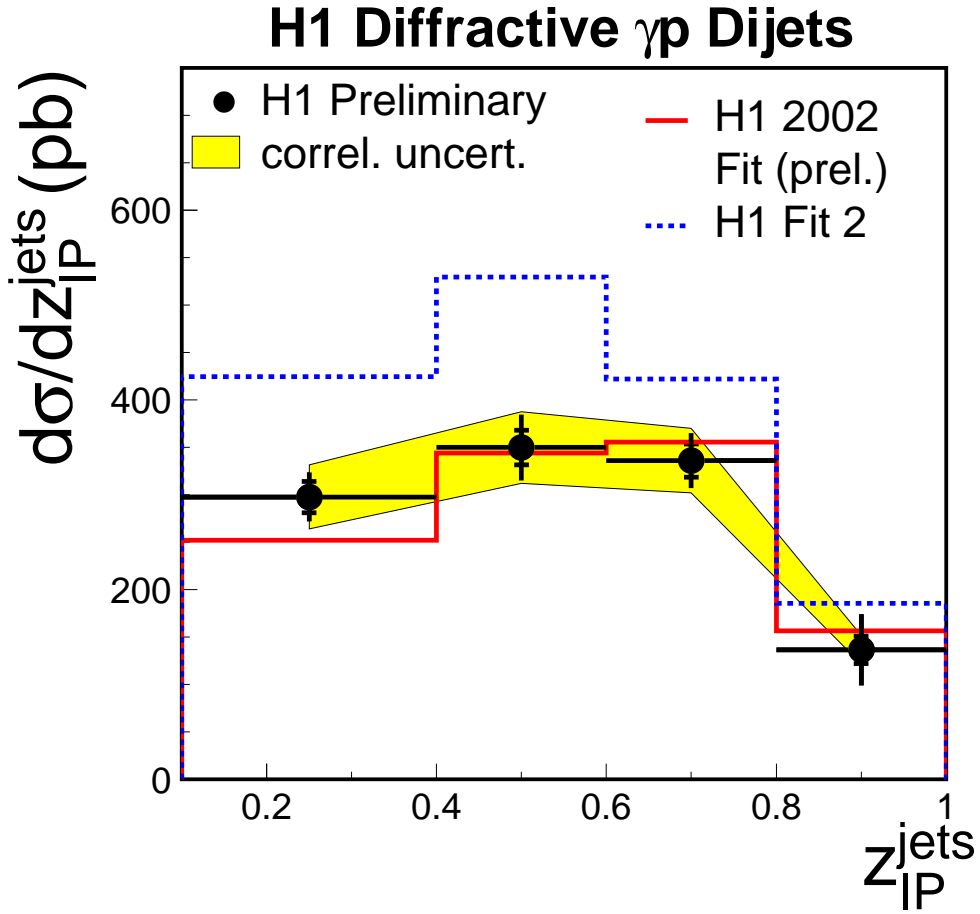


Figure 2: Cross section differential in z_{IP}^{jets} for the diffractive production of 2 jets in the photo-production kinematic region specified in Table 1. The inner error bars represent the statistical errors and the outer error bars the quadratic sum of the statistical and uncorrelated systematic errors. The shaded band shows correlated normalisation uncertainties of the data. Also shown are two predictions of the RAPGAP model with LO diffractive parton densities from the new H1 2002 fit (solid histogram) and the H1 fit 2 (dashed histogram). For both predictions, the LO GRV parton distributions of the photon are used.

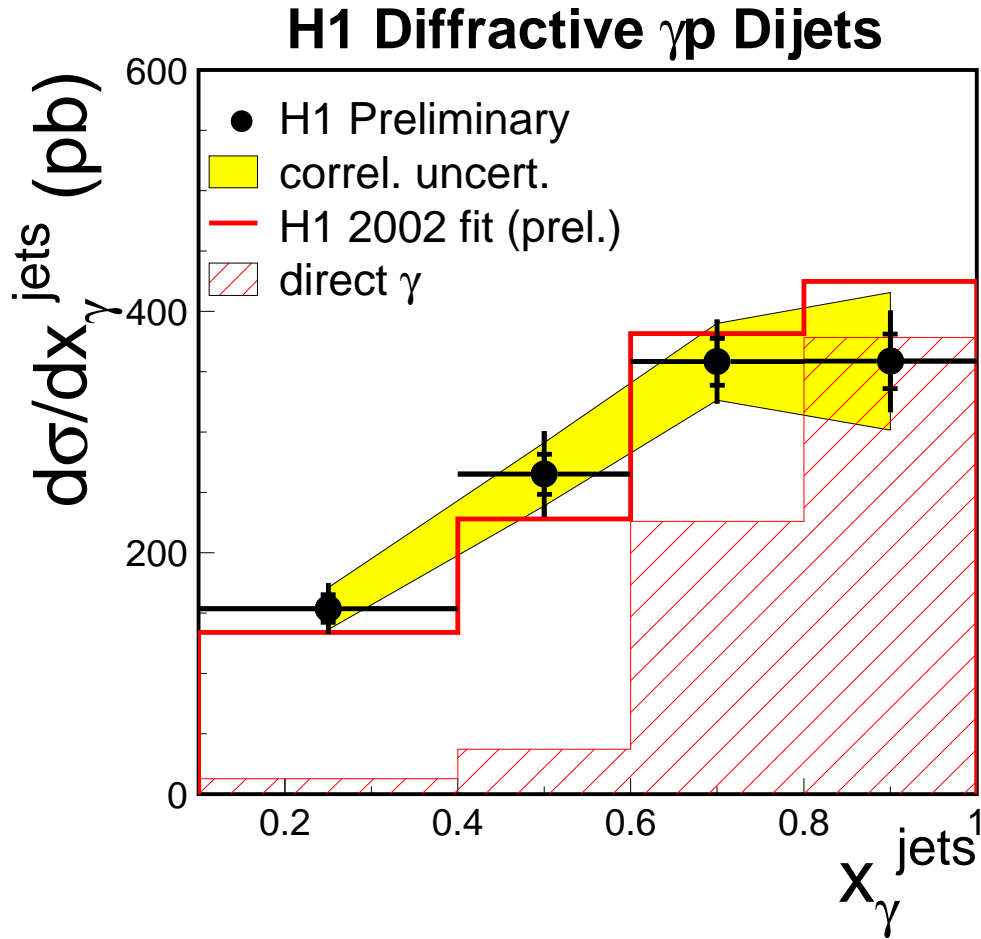


Figure 3: Cross section differential in x_γ^{jets} for the diffractive production of 2 jets in the photo-production kinematic region specified in Table 1. The inner error bars represent the statistical errors and the outer error bars the quadratic sum of the statistical and uncorrelated systematic errors. The shaded band shows correlated normalisation uncertainties of the data. Also shown is the prediction of the RAPGAP model with LO diffractive parton densities from the new H1 2002 fit. The direct photon contributions (boson gluon fusion and QCD compton) are indicated by the hatched histogram. The LO GRV parton distributions of the photon are used.

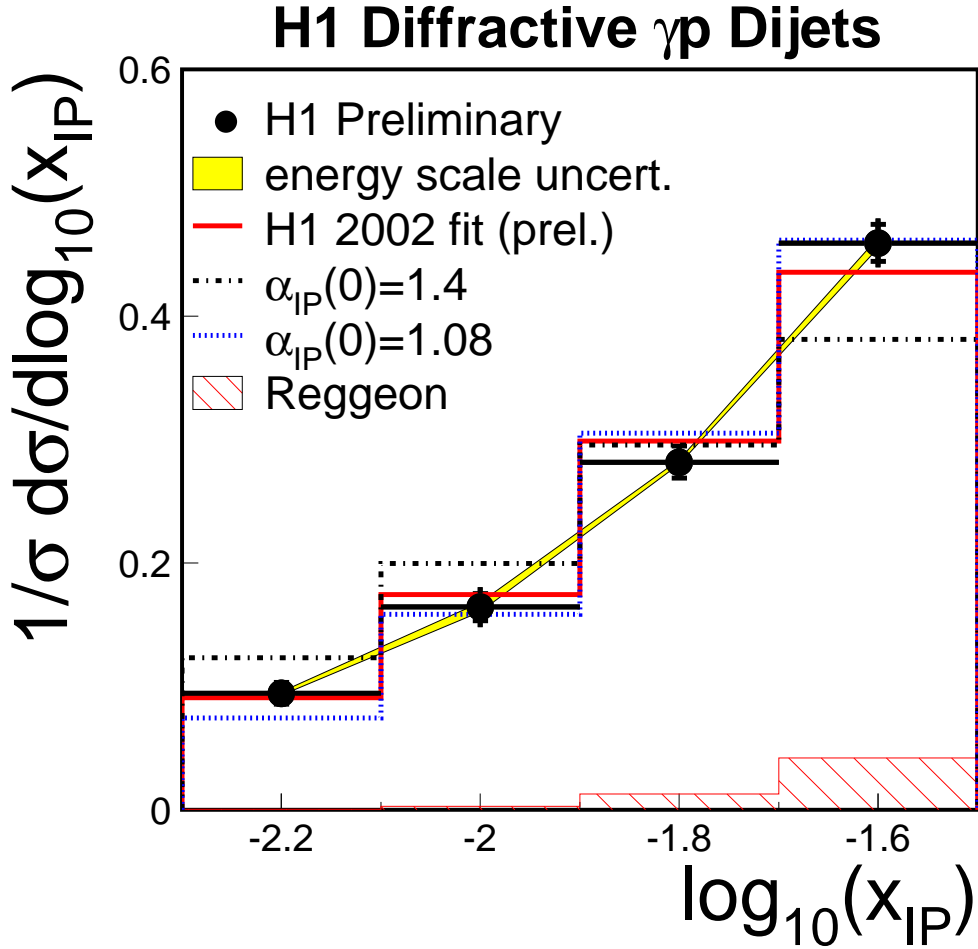


Figure 4: Normalised cross section differential in x_{IP} for the diffractive production of 2 jets in the photoproduction kinematic region specified in Table 1. The inner error bars represent the statistical errors and the outer error bars the quadratic sum of the statistical and uncorrelated systematic errors. The shaded band shows the uncertainty of the data resulting from the uncertainty of the calorimeter energy scale. Also shown are predictions of the RAPGAP model with LO diffractive parton densities from the H1 2002 fit, with intercepts $\alpha_{IP}(0)=1.17$, labelled ‘H1 2002 fit (prel.),’ $\alpha_{IP}(0)=1.08$ (dotted histogram), and $\alpha_{IP}(0)=1.4$ (dash-dotted histogram). The sub-leading Reggeon contribution is shown as the hatched histogram. The LO GRV parton distributions of the photon are used.

H1 Diffractive γp Dijets

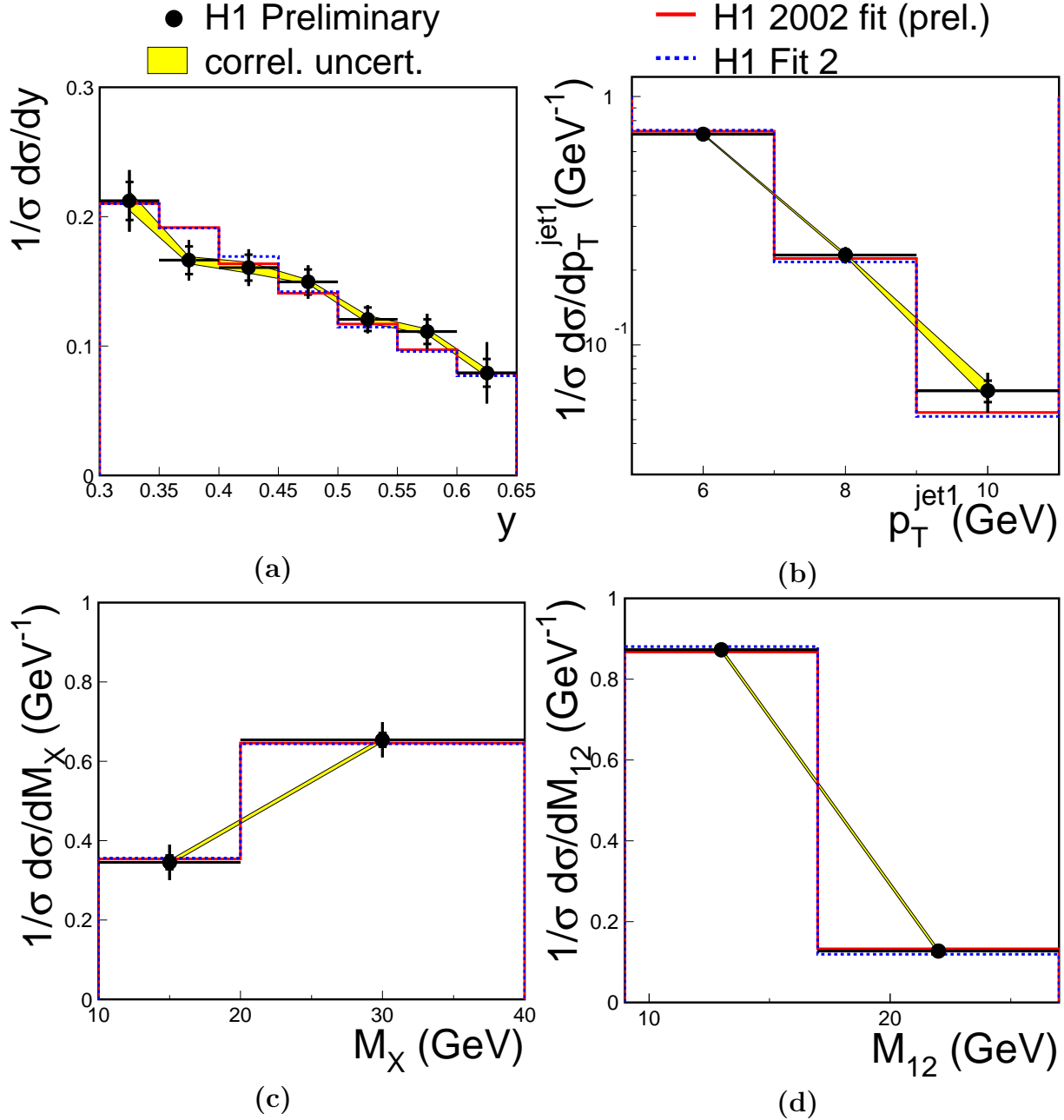


Figure 5: Normalised differential cross sections for the diffractive production of 2 jets in the photoproduction kinematic region specified in Table 1: (a) y , (b) p_T^{jet1} , (c) M_X and (d) M_{12} . The inner error bars represent the statistical errors and the outer error bars the quadratic sum of the statistical and uncorrelated systematic errors. The shaded bands show correlated normalisation uncertainties of the data. Also shown are two predictions of the RAPGAP model with LO diffractive parton densities from the new H1 2002 fit (solid histogram) and the H1 fit 2 (dashed histogram). For both predictions, the LO GRV parton distributions of the photon are used.

H1 Diffractive γp Dijets

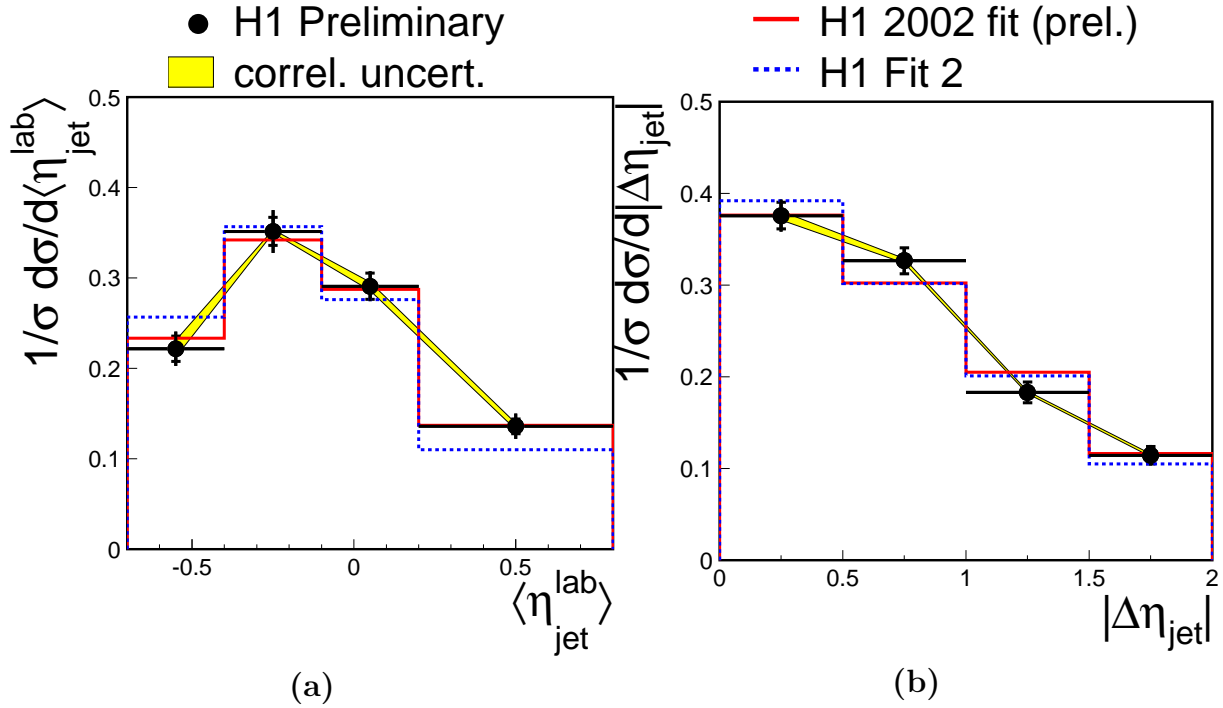


Figure 6: Normalised differential cross sections for the diffractive production of 2 jets in the photoproduction kinematic region specified in Table 1: (a) $\langle\eta_{\text{jet}}^{\text{lab}}\rangle$ and (b) $|\Delta\eta_{\text{jet}}|$. The inner error bars represent the statistical errors and the outer error bars the quadratic sum of the statistical and uncorrelated systematic errors. The shaded bands show correlated normalisation uncertainties of the data. Also shown are two predictions of the RAPGAP model with LO diffractive parton densities from the new H1 2002 fit (solid histogram) and the H1 fit 2 (dashed histogram). For both predictions, the LO GRV parton distributions of the photon are used.